VIP Superconductivity and Ferromagnetism Very Important Paper

DOI: 10.1002/anie.201407756

# Coexistence of 3d-Ferromagnetism and Superconductivity in $[(Li_{1-x}Fe_x)OH](Fe_{1-y}Li_y)Se$**

*Ursula Pachmayr, Fabian Nitsche, Hubertus Luetkens, Sirko Kamusella, Felix Brückner, Rajib Sarkar, Hans-Henning Klauss, and Dirk Johrendt**

***Abstract:*** *Superconducting $[(Li_{1-x}Fe_x)OH](Fe_{1-y}Li_y)Se$ ($x \approx 0.2$, $y \approx 0.08$) was synthesized by hydrothermal methods and characterized by single-crystal and powder X-ray diffraction. The structure contains alternating layers of anti-PbO type $(Fe_{1-y}Li_y)Se$ and $(Li_{1-x}Fe_x)OH$. Electrical resistivity and magnetic susceptibility measurements reveal superconductivity at 43 K. An anomaly in the diamagnetic shielding indicates ferromagnetic ordering near 10 K while superconductivity is retained. The ferromagnetism is from the iron atoms in the $(Li_{1-x}Fe_x)OH$ layer. Isothermal magnetization measurements confirm the superposition of ferromagnetic and superconducting hysteresis. The internal ferromagnetic field is larger than the lower, but smaller than the upper critical field of the superconductor. The formation of a spontaneous vortex phase where both orders coexist is supported by $^{57}$Fe-Mössbauer spectra, $^{7}$Li-NMR spectra, and μSR experiments.*

Superconductivity expels magnetic flux from the interior of a solid, while ferromagnetism generates it, thus these phenomena are antagonistic. Moreover, ferromagnetic order is usually detrimental to superconductivity because strong internal fields from aligned moments break Cooper pairs. Nevertheless, both phenomena are not mutually exclusive in all cases. After early investigations of alloys with magnetic rare-earth atoms diluted in superconducting lanthanum metal,[1] the first superconductors with spatially ordered arrays of magnetic atoms were the metallic molybdenum sulfides $RE Mo_6S_8$ ($RE$ = rare earth element), referred to as the Chevrel phases.[2,3] Among them, compounds with the strongly magnetic rare-earth elements Tb–Er have superconducting critical temperatures ($T_c$) around 2 K, and enter magnetically ordered states between 15 mK and 5 mK.[4,5] A further example is $ErRh_4B_4$ where ferromagnetism destroys superconductivity at 1 K, while co-existence with antiferromagnetic ordering has been found in the borocarbides $RENi_2B_2C$[6,7] and the ruthenate $RuSr_2GdCu_2O_8$.[8] Recently, the co-existence of superconductivity and ferromagnetic ordering of $Eu^{2+}$ ions in the iron arsenides $EuFe_2(As_{1-x}P_x)_2$ and $Eu(Fe_{1-x}Ru_x)_2As_2$ has been reported.[9–11] Such materials where the ferromagnetic ordering temperature $T_{fm}$ is below $T_c$ are called ferromagnetic superconductors. Therein, both phenomena are usually spatially decoupled, and do not interact directly in the sense that the same electrons are responsible for both. The situation in which the same electrons are responsible for both phenomena is discussed in superconducting ferromagnets with $T_{fm} > T_c$. In these materials the superconducting state emerges in a ferromagnetic metal (usually at mK temperatures), which gives evidence for exotic mechanisms, such as spin triplet pairing, for example in $UGe_2$ or URhGe which have been intensively studied.[12–14]

To date the extremely low temperatures, as well as the inertness of the rare-earth 4f shell hardly allowed chemical manipulation of these quite fascinating phenomena. This would be different if the ferromagnetic ordering emerges from d-elements, where the magnetic state is much more susceptible to the chemical environment. Materials where superconductivity coexists with 3d-ferromagnetism in a bulk phase are unknown to our knowledge.[15,16] Herein we report the synthesis, crystal structure, and basic physical properties of the ferromagnetic superconductor $[(Li_{1-x}Fe_x)OH](Fe_{1-y}Li_y)Se$, in which magnetic ordering emerges from iron ions in the hydroxide layer at 10 K, which is sandwiched between iron selenide layers providing superconductivity up to 43 K.

Polycrystalline samples of $[(Li_{1-x}Fe_x)OH](Fe_{1-y}Li_y)Se$ were synthesized under hydrothermal conditions using a modified procedure given in Ref. [17]. Figure 1 shows an

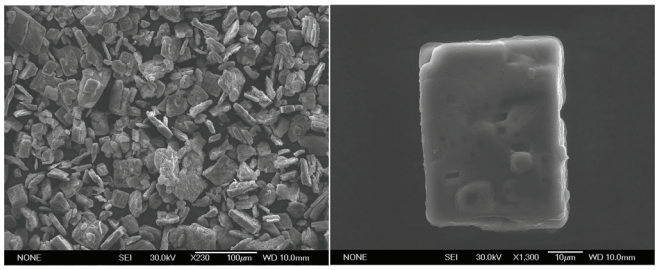

***Figure 1.*** Left: SEM image of a $[(Li_{1-x}Fe_x)OH](Fe_{1-y}Li_y)Se$ sample. Right: plate-like single crystal.

[*] U. Pachmayr, F. Nitsche, Prof. Dr. D. Johrendt
Department Chemie, Ludwig-Maximilians-Universität München
Butenandtstrasse 5–13 (Haus D)
81377 München (Germany)
E-mail: johrendt@lmu.de

Dr. H. Luetkens
Paul Scherrer Institut PSI
5232 Villigen (Switzerland)

S. Kamusella, F. Brückner, Dr. R. Sarkar, Prof. Dr. H.-H. Klauss
Institut für Festkörperphysik, Technische Universität Dresden
01062 Dresden (Germany)

[**] We thank the German Research Foundation (DFG) for financial support of this work within SPP1458 and GRK1621. U.P. and F.N. were supported by the FP7 European project SUPER-IRON (No. 283204).

Supporting information for this article is available on the WWW under http://dx.doi.org/10.1002/anie.201407756.

  

electron microscope image of the sample and a typical plate-like crystal. A small specimen ($50 \times 40 \times 5\ \mu m^3$) was selected for the X-ray single crystal analysis. First structure refinements using the data of $LiFeO_2Fe_2Se_2$ given by Lu et al.[17] as starting parameters were not satisfying. A closer inspection revealed residual electron density at about 75 pm below the oxygen atoms which indicated additional hydrogen. Furthermore the $U_{33}$ component of the thermal displacement ellipsoid at the Fe/Li site was too large, which required a split position with Li shifted off the center of the oxygen tetrahedra by 40 pm along the *c*-direction. Attempts to find an ordered model by twinning and/or symmetry reduction failed. Finally we detected a slight deficiency at the iron site in the FeSe layer. X-ray diffraction cannot distinguish between iron vacancies or a possible Fe/Li mixed site. Since Li-NMR spectroscopy shows two Li sites in the structure, we interpret the deficiency as Fe/Li mixing with approximately 8% Li. Using this model, the structure refinements rapidly converged to small residuals ($R1 = 0.016$). The crystallographic parameters are compiled in Table S1 of the Supporting Information. In the following we denote iron in the hydroxide layer as $Fe^a$ and in the FeSe layer as $Fe^b$. By using these crystal data we were able to perform a Rietveld fit of the X-ray powder pattern, which revealed the identical structure and confirmed that the sample is free from impurities within the sensitivity of laboratory X-ray powder diffraction. The crystal structure of $[(Li_{1-x}Fe_x)OH](Fe_{1-y}Li_y)Se$ is depicted in the insert of Figure 2. Along the *c*-axis *anti*-PbO type layers of lithium-iron-hydroxide alternate with FeSe-layers. Unlike $LiFeO_2Fe_2Se_2$[17] our compound is not an oxide but a hydroxide, where positively polarized hydrogen atoms point towards the negatively polarized selenium of the FeSe layer. The structure of the $(Li_{1-x}Fe_x)OH$ layer is quite similar to LiOH itself, which likewise crystallizes in the *anti*-PbO-type.[18]

The Se-Fe-Se bond angles of the $FeSe_4$ tetrahedra are almost identical to those in binary β-FeSe,[19] while the Fe–Se bond lengths (241.4 pm) are slightly longer than in β-FeSe (239.5 pm). Thus no significant changes apply to the structure of the FeSe layer in $[(Li_{1-x}Fe_x)OH](Fe_{1-y}Li_y)Se$, however, the tiny elongation of the Fe–Se bonds may already influence the electronic properties. The situation in the hydroxide layer is more difficult. Iron is in a flattened tetrahedron of oxygen atoms with a Fe–O distance of 201.6 pm. This matches the sum of the ionic radii[20] if iron is $Fe^{2+}$ (203 pm), but not if iron is $Fe^{3+}$ (189 pm). Thus we suggest the presence of $Fe^{2+}$ in the hydroxide layer, even though a tetrahedral coordination is rather unusual. Lithium in the center of the flat oxygen tetrahedron would have Li–O separation of 201.6 pm, significantly longer than the 196 pm in LiOH.[21] We suggest that this is the reason why Li is shifted along *c*, however, the Li position is not precise owing to the low scattering power. This is even more the case for the hydrogen atom, where the refined O–H distance is 72(8) pm. Given the large error and the fact that X–H bond lengths from X-ray diffraction are usually underestimated by at least 10%, we are not that far from the O–H distance in LiOH which was determined to be 89 pm using neutron diffraction.[18]

The composition obtained from X-ray diffraction is $(Li_{0.795(5)}Fe_{0.205(5)})OH(Fe_{0.915(4)}Li_{0.085(4)})Se$. However, the true errors of the stoichiometric indices are certainly higher and rather in the range of about ±10%. Within this range, energy dispersive X-ray spectroscopy (EDX) measurements confirm the contents of iron, selenium, and oxygen. Lithium was determined by inductively coupled plasma (ICP) analysis and hydrogen by elementary analysis to be 0.8(3) wt% in general agreement with the expected 0.613 wt%.

Figure 3 shows electrical transport and low-field magnetic susceptibility measurements of the $[(Li_{1-x}Fe_x)OH](Fe_{1-y}Li_y)Se$ sample. The resistivity is relatively high at 300 K and weakly temperature dependent until it drops abruptly at 43 K. Zero resistivity is reached below 25 K. The superconducting transition is confirmed by the magnetic susceptibility which becomes strongly diamagnetic below 40 K in a 30 mT field. However, the low-temperature susceptibility behaves quite unusual. After zero-field cooling (zfc, Figure 3) the value starts strongly negative according to the shielding effect, and first increases with temperature until a maximum is reached at 10 K, then decreases again until 18 K, and finally increases steeply to zero as the temperature approaches $T_c$. In field-cooled mode (fc, Figure 3), the susceptibility becomes slightly negative below 40 K owing to the Meissner–Ochsenfeld effect, but increases again to

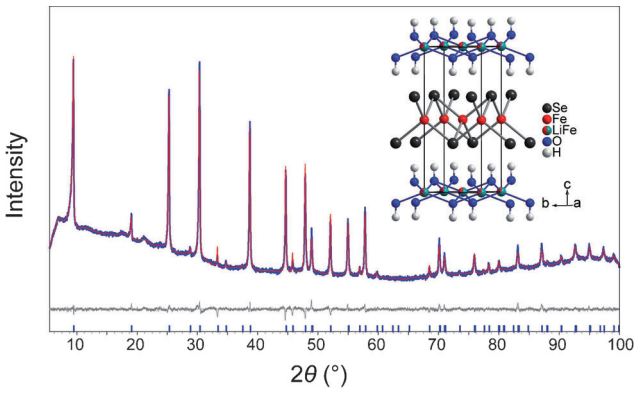


***Figure 2.*** X-ray powder pattern (blue) with Rietveld-fit (red) and difference curve (gray). Insert: crystal structure of $[(Li_{1-x}Fe_x)OH](Fe_{1-y}Li_y)Se$.

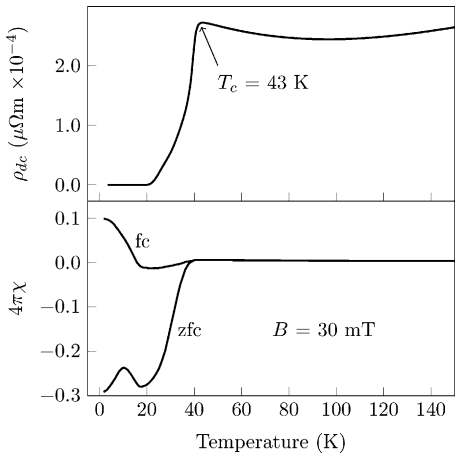


***Figure 3.*** Top: dc resistivity of the $[(Li_{1-x}Fe_x)OH](Fe_{1-y}Li_y)Se$ sample. Bottom: dc magnetic susceptibility.

positive values at lower temperatures. Remarkably, the diamagnetism of the superconductor competes with strong paramagnetism which emerges below 18 K. The paramagnetism dominates in the fc mode, in which the diamagnetic contribution arising from the Meissner effect is weak. Thus actually no Meissner phase exists at the lowest temperatures. In contrast in zfc mode the diamagnetic shielding is much stronger than the paramagnetic contribution. Note that the resistivity remains zero at low temperatures, which means that the emerging paramagnetic field is not strong enough to destroy the superconductivity.

The magnetic susceptibility experiment suggests that superconductivity coexists with ferromagnetic ordering which emerges near 18 K, well below the critical temperature of 43 K. Figure 4 shows the isothermal magnetization measured at 1.8 K. The typical ferromagnetic hysteresis is superimposed by the magnetization known for hard type-II superconductors.[22,23] This becomes obvious if the approximate ferromagnetic contribution (dashed line in Figure 4) is subtracted. The resulting curve (inset in Figure 4) is typical for a superconductor which is partially penetrated by magnetic flux lines (mixed or Shubnikov phase). Some flux becomes trapped by vortex pinning, therefore we detect non-zero magnetization even at zero external field ($B=0$). The upper critical field of the superconductor is not reached at 5 T, where the magnetization makes a typical jump because the sign of the field change ΔB reverses, and thus the directions of the shielding currents are also reversed.

Unlike to the Chevrel phases or $ErRh_4B_4$ where the ferromagnetism destroys superconductivity, we observe the rare case where both phenomena can coexist because the ferromagnetic dipole field is smaller than the upper critical field of the superconductor. Given that the magnetization emerges inside the sample owing to ferromagnetic ordering and not because of an external field, our material is in a so-called spontaneous vortex state. This is a new state of matter, where both orders coexist because the combined state has a lower free energy.[24] Similar behavior has been suggested in $EuFe_2(As_{1-x}P_x)_2$ where ferromagnetic ordering of $Eu^{2+}$ ($4f^7$) coexists with superconductivity.[9,11] In our case the ferromagnetism originates from the iron atoms in the $(Li_{1-x}Fe_x)OH$ layer (see below), thus $[(Li_{1-x}Fe_x)OH](Fe_{1-y}Li_y)Se$ is to our knowledge the first example where superconductivity coexists with 3d ferromagnetism in a bulk material, and moreover at the highest temperatures to date.

The $^{57}Fe$ Mössbauer spectrum (insert in Figure 5) consists of two doublets with an intensity ratio 0.9:0.1 in agreement with $Fe^b$ in the FeSe and $Fe^a$ in the hydroxide layers. The isomer shift of approximately 0.8 mm s$^{-1}$ for $Fe^a$ is typical for $Fe^{2+}$ in a $S=4/2$ state. The $Fe^a$ doublet considerably broadens below $T_{fm}\approx 10$ K which can be described by a hyperfine field of 3 T at 2.1 K. A small stray field of 0.4 T arising most probably from these ordered moments broadens the doublet at the $Fe^b$ site in the FeSe layer. The remanence of the internal fields confirms the ferromagnetism. A third small subspectrum supports the asymmetry of the spectrum and suggests $Fe^b$ sites in the FeSe layer with Li neighbors at the iron position.

Zero field muon spin rotation (μSR) data confirm the homogeneity of the sample as well as ferromagnetic ordering below $T_{fm}\approx 10$ K (Figure 5). The magnetism develops gradually while the whole sample is ferromagnetic at 1.5 K. A non-magnetic fraction senses enhanced damping as a result of static fields from the magnetically ordered layer below 10 K. Reducing the field cooled flux of 200 G to 170 G we can successfully demonstrate bulk superconductivity by pinning nearly 40 % of the flux at 15 K, confirmed by transverse field (TF) data at 200 G. Cooling the sample from 40 K to 15 K a considerable damping of the precession signal in more than 40 % of the sample is induced, most probably a result of flux line lattice formation and not ferromagnetism. However both TF and pinning experiments at 1.5 K indicated, that superconducting volume fractions are reduced by ferromagnetism.

High-resolution[25] $^7Li$ NMR spectra taken at 36 MHz show two signal fractions originating from two Li sites (Figure 6), while the respective characteristic $T_1$ relaxation times are spread over approximately three orders of magni-

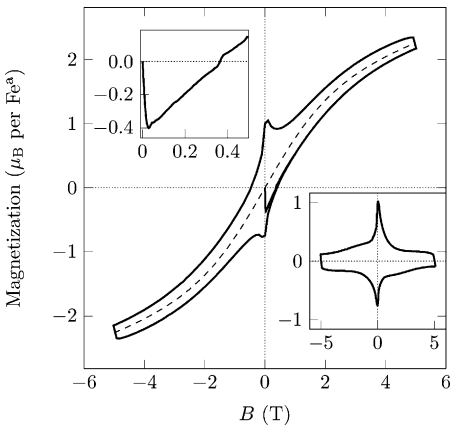


***Figure 4.*** Isothermal magnetization at 1.8 K. Left inset: magnification of the low-field part showing the initial curve. Right inset: magnetization after subtraction of the approximate ferromagnetic contribution (dashed line in the main plot).

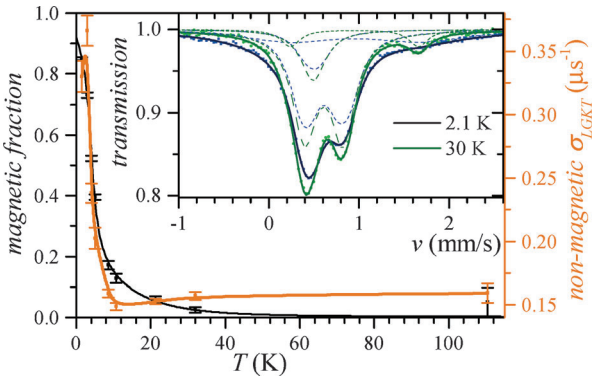


***Figure 5.*** Magnetic volume fraction obtained by zero-field μSR shows that almost the whole sample is ruled by ferromagnetism at low temperatures. The increase of the static relaxation rate $\sigma_{LGKT}$ is due to the ferromagnetic stray field in the non-magnetic sample fraction. $^{57}Fe$ Mössbauer spectra detect two iron sites and demonstrate that magnetism arises from iron in the hydroxide layer, whereas the FeSe layer only senses stray fields.

  

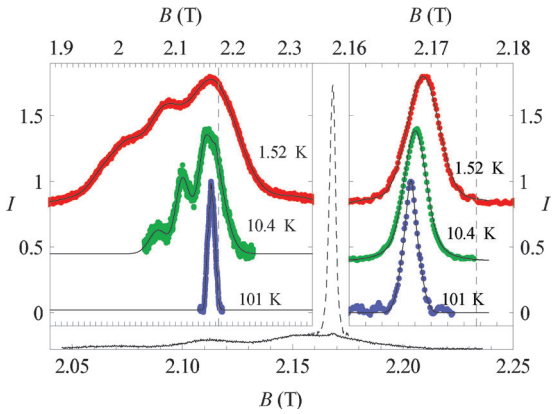


***Figure 6.*** $^{7}$Li NMR spectra of $[(Li_{1-x}Fe_x)OH](Fe_{1-y}Li_y)Se$. Outer graph: NMR spectra at 10 K with a short repetition time (solid line) and with a long repetition time (dashed line). Left inset: temperature dependency of the broad fraction. Right inset: temperature dependency of the narrow fraction.

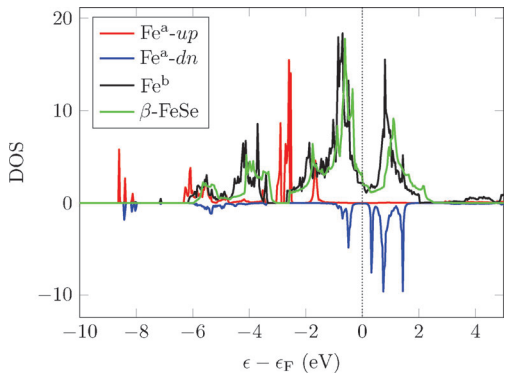


***Figure 7.*** Electronic density of states (DOS) contributions of the iron atoms. Red/blue: Magnetic Fe$^a$ atoms in the hydroxide layer; black: non-magnetic Fe$^b$ atoms in the FeSe layer; green: Fe-atoms in binary β-FeSe for comparison.

tude. The main fraction is broad and relaxes very fast. At low temperatures, the spectrum splits into three broadened peaks. In contrast to that, the other fraction is a narrow line and relaxes very slowly. The spectrum shifts and its shape broadens slightly at low temperatures. Comparing the intensities of both spectral fractions, we assign the broad spectrum to lithium in the $(Li_{1-x}Fe_x)OH$ layer, which is in line with the Mössbauer results. The close proximity to the magnetic Fe$^a$ atoms leads to broadening and a large shift. Because the Fe$^a$ atoms are statistically distributed, different Li-surroundings produce a complex peak structure at low temperatures. The narrow spectrum is assigned to the Li at the Fe$^b$ sites in the non-magnetic FeSe layer. The small shift and broadening at low temperatures is due to stray fields and vanishing Pauli magnetism in the superconducting phase.

DFT band-structure calculations with an ordered model of $[(Li_{0.8}Fe^{a}_{0.2})OH]Fe^{b}Se$ according to $[Li_4Fe^{a}(OH)_5](Fe^{b}Se)_5$ were carried out. First the atomic coordinates of a $\sqrt{5}a \times \sqrt{5}a$ superstructure were allowed to relax, then we tried different magnetic ordering patterns. No magnetic ground state with non-zero moments at the Fe$^b$ site in the FeSe layer could be obtained. On the other hand, ferromagnetic ordering of the moments at the Fe$^a$ site in the hydroxide layer lowered the total energy by 41 kJ mol$^{-1}$ with a magnetic moment of 3.5 $\mu_B$ per Fe$^a$. Antiferromagnetic ordering resulted in the same stabilization, thus our model cannot distinguish between ordering patterns, but it definitely shows that magnetism emerges from iron atoms in the hydroxide layer.

Figure 7 shows the contributions of the different iron atoms to the electronic density of states (DOS). The magnetic exchange splitting of the Fe$^a$ states is clearly discernible, while the states of the non-magnetic Fe$^b$ sites remain almost exactly as in binary β-FeSe (green line in Figure 7). Moreover, the Fermi-level is located in a gap of the magnetic Fe$^a$ states. This means that the electronic systems of the individual layers interact very weakly, and that the typical Fermi-surface topology known from other iron based superconductors[26] is not disturbed by the presence of the hydroxide layer. Nevertheless the hydroxide layer acts as an electron reservoir. Formally 0.2 electrons are transferred from the hydroxide to the selenide layer according to $[(Li_{0.8}Fe^{2+}_{0.2})OH]^{0.2+}(FeSe)^{0.2-}$. This is also evident from the small shift of the Fe$^b$ states (black line in Figure 7) to lower energies relatively to β-FeSe. We suggest that this electron doping of the FeSe layer is mainly responsible for the enormous increase of $T_c$ in our compound (43 K) in comparison to β-FeSe (8 K). Similar electron transfers of approximately 0.2 e$^-$/FeSe have recently been reported for other intercalated iron selenides, among them $Li_x(NH_2)_y(NH_3)_{1-y}Fe_2Se_2$ ($T_c = 43$ K),[27,28] $K_xFe_2Se_2$ ($T_c = 32$ K),[29] $Na_xFe_2Se_2$ ($T_c \approx 46$ K),[30,31] and $Li_x(C_2H_8N_2)_yFe_{2-z}Se_2$ ($T_c \approx 45$ K).[32]

In conclusion, we have shown that superconductivity below $T_c = 43$ K coexists with ferromagnetism below $T_{fm} \approx 10$ K in $[(Li_{1-x}Fe_x)OH](Fe_{1-y}Li_y)Se$ synthesized under hydrothermal conditions. The layered crystal structure consists of ferromagnetic $(Li_{1-x}Fe_x)OH$ and superconducting $(Fe_{1-y}Li_y)Se$ layers each with *anti*-PbO-type structures. Both physical phenomena are spatially separated, but the internal dipole field of the ferromagnet acts on the superconductor, which suggests the existence of a special state of matter called a spontaneous vortex phase. The $^{57}$Fe-Mössbauer spectroscopy, $^{7}$Li-NMR, and μSR measurements consistently support this conclusion. This rare phenomenon was so far confined to f-shell magnetism, while in our compound superconductivity coexists with 3d-ferromagnetism for the first time, and moreover at the highest temperatures to date. In contrast to the chemically inert f-shells, 3d-magnetism is much more susceptible to the chemical environment, which opens new avenues for chemical modifications that can now directly couple to the magnetic and superconducting properties, thus allowing broader studies of such coexistence phenomena in the future.

### *Experimental Section*

Polycrystalline samples of $[(Li_{1-x}Fe_x)OH](Fe_{1-y}Li_y)Se$ were synthesized under hydrothermal conditions using a modified procedure given in Ref. [17]. Iron metal (99.9 %; 0.0851 g), Selenourea (99 %; 0.5 g ) and $LiOH{\cdot}H_2O$ (3 g) were mixed with distilled water (10 mL). The starting mixtures were

  

tightly sealed in a teflon-lined steel autoclave (50 mL) and heated at 150 °C for 8 days. The shiny lamellar precipitates obtained were separated by centrifugation, and washed several times with distilled water and ethanol. Afterwards, the polycrystalline products were dried at room temperature under dynamic vacuum and stored at −25 °C under argon atmosphere.

X-ray powder diffraction was carried out using a Huber G670 diffractometer with Cu-K$\alpha_1$ radiation ($\lambda = 154.05$ pm) and Ge-111 monochromator. Structural parameters were obtained by Rietveld refinement using the software package TOPAS.[33] Single-crystal analysis was performed on a Bruker D8-Quest diffractometer (Mo-K$\alpha_1$, $\lambda = 71.069$ pm, graphite monochromator). The structure was solved and refined with the Jana2006 program package.[34] Chemical compositions were additionally determined by energy-dispersive X-ray analysis (EDX) as well as by chemical methods using ICP-AAS and elemental analysis. Magnetic properties were examined with a Quantum Design MPMS-XL5 SQUID magnetometer, whereas temperature-dependent resistivity measurements were carried out using a standard four-probe method.

$^{57}$Fe-Mössbauer spectroscopy was performed with a standard Wissel setup in transmission geometry using a Co/Rh source. μSR experiments were carried out with the GPS spectrometer at the πM3.2 beamline of the Swiss Muon Source at the Paul Scherrer Institut in Villigen, Switzerland. $^7$Li NMR spectra were taken at several temperatures using the Fourier-transformation field-sweep method.

Electronic structure calculations were performed using the Vienna ab initio simulation package (VASP),[35,36] which is based on density functional theory (DFT) and plane-wave basis sets. Projector-augmented waves (PAW)[37] were used and contributions of correlation and exchange were treated in the generalized-gradient approximation (GGA) as described by Perdew, Burke, and Ernzerhof.[38]

Received: July 30, 2014
Revised: August 25, 2014
Published online: October 7, 2014

**Keywords:** ferromagnetism · iron selenides · structure elucidations · superconductivity

[1] B. T. Matthias, H. Suhl, E. Corenzwit, *Phys. Rev. Lett.* **1958**, *1*, 449.
[2] R. Chevrel, M. Sergent, J. Prigent, *J. Solid State Chem.* **1971**, *3*, 515.
[3] B. T. Matthias, M. Marezio, E. Corenzwit, A. S. Cooper, H. E. Barz, *Science* **1972**, *175*, 1465.
[4] M. Ishikawa, Ø. Fischer, *Solid State Commun.* **1977**, *24*, 747–751.
[5] J. W. Lynn, D. E. Moncton, W. Thomlinson, G. Shirane, R. N. Shelton, *Solid State Commun.* **1978**, *26*, 493.
[6] W. A. Fertig, D. C. Johnston, L. E. DeLong, R. W. McCallum, M. B. Maple, B. T. Matthias, *Phys. Rev. Lett.* **1977**, *38*, 987.
[7] J. W. Lynn, S. Skanthakumar, Q. Huang, S. K. Sinha, Z. Hossain, L. C. Gupta, R. Nagarajan, C. Godart, *Phys. Rev. B* **1997**, *55*, 6584.
[8] J. W. Lynn, B. Keimer, C. Ulrich, C. Bernhard, J. L. Tallon, *Phys. Rev. B* **2000**, *61*, 14964.
[9] G. Cao, S. Xu, Z. Ren, S. Jiang, C. Feng, Z. a. Xu, *J. Phys. Condens. Matter* **2011**, *23*, 464204.
[10] W.-H. Jiao, J.-K. Bao, Q. Tao, H. Jiang, C.-M. Feng, Z.-A. Xu, G.-H. Cao, *J. Phys. Conf. Ser.* **2012**, *400*, 022038.
[11] S. Nandi, W. T. Jin, Y. Xiao, Y. Su, S. Price, D. K. Shukla, J. Strempfer, H. S. Jeevan, P. Gegenwart, T. Brückel, *Phys. Rev. B* **2014**, *89*, 014512.
[12] S. S. Saxena, P. Agarwal, K. Ahilan, F. M. Grosche, R. K. W. Haselwimmer, M. J. Steiner, E. Pugh, I. R. Walker, S. R. Julian, P. Monthoux, G. G. Lonzarich, A. Huxley, I. Sheikin, D. Braithwaite, J. Flouquet, *Nature* **2000**, *406*, 587.
[13] A. Huxley, I. Sheikin, E. Ressouche, N. Kernavanois, D. Braithwaite, R. Calemczuk, J. Flouquet, *Phys. Rev. B* **2001**, *63*, 144519.
[14] D. Aoki, A. Huxley, E. Ressouche, D. Braithwaite, J. Flouquet, J. P. Brison, E. Lhotel, C. Paulsen, *Nature* **2001**, *413*, 613.
[15] T. Herrmannsdörfer, R. Skrotzki, J. Wosnitza, D. Köhler, R. Boldt, M. Ruck, *Phys. Rev. B* **2001**, *83*, 140501.
[16] X. Zhu, H. Lei, C. Petrovic, Y. Zhang, *Phys. Rev. B* **2012**, *86*, 024527.
[17] X. F. Lu, N. Z. Wang, G. H. Zhang, X. G. Luo, Z. M. Ma, B. Lei, F. Q. Huang, X. H. Chen, *Phys. Rev. B* **2014**, *89*, 020507.
[18] H. Dachs, *Z. Kristallogr.* **1959**, *112*, 60.
[19] T. M. McQueen, Q. Huang, V. Ksenofontov, C. Felser, Q. Xu, H. Zandbergen, Y. S. Hor, J. Allred, A. J. Williams, D. Qu, J. Checkelsky, N. P. Ong, R. J. Cava, *Phys. Rev. B* **2009**, *79*, 014522.
[20] R. D. Shannon, C. T. Prewitt, *Acta Crystallogr. Sect. B* **1969**, *25*, 925.
[21] S. Mair, *Acta Crystallogr. Sect. A* **1978**, *34*, 542.
[22] W. Buckel, R. Kleiner, *Superconductivity. Fundamentals and Applications*, *Vol. 6*, Wiley-VCH, Weinheim, **2004**.
[23] C. P. Bean, *Phys. Rev. Lett.* **1962**, *8*, 250.
[24] H. S. Greenside, E. I. Blount, C. M. Varma, *Phys. Rev. Lett.* **1981**, *46*, 49.
[25] G. J. Rees et al., *Phys. Chem. Chem. Phys.* **2013**, *15*, 17195.
[26] M. Sunagawa, T. Ishiga, K. Tsubota, T. Jabuchi, J. Sonoyama, K. Iba, K. Kudo, M. Nohara, K. Ono, H. Kumigashira, T. Matsushita, M. Arita, K. Shimada, H. Namatame, M. Taniguchi, T. Wakita, Y. Muraoka, T. Yokoya, *Sci. Rep.* **2014**, *4*, 4381.
[27] M. Burrard-Lucas, D. G. Free, S. J. Sedlmaier, J. D. Wright, S. J. Cassidy, Y. Hara, A. J. Corkett, T. Lancaster, P. J. Baker, S. J. Blundell, S. J. Clarke, *Nat. Mater.* **2013**, *12*, 15.
[28] S. J. Sedlmaier, S. J. Cassidy, R. G. Morris, M. Drakopoulos, C. Reinhard, S. J. Moorhouse, D. O'Hare, P. Manuel, D. Khalyavin, S. J. Clarke, *J. Am. Chem. Soc.* **2014**, *136*, 630.
[29] S. V. Carr, D. Louca, J. Siewenie, Q. Huang, A. Wang, X. Chen, P. Dai, *Phys. Rev. B* **2014**, *89*, 134509.
[30] T. P. Ying, X. L. Chen, G. Wang, S. F. Jin, T. T. Zhou, X. F. Lai, H. Zhang, W. Y. Wang, *Sci. Rep.* **2012**, *2*, 426.
[31] T. Ying, X. Chen, G. Wang, S. Jin, X. Lai, T. Zhou, H. Zhang, S. Shen, W. Wang, *J. Am. Chem. Soc.* **2013**, *135*, 2951.
[32] T. Hatakeda, T. Noji, T. Kawamata, M. Kato, Y. Koike, *J. Phys. Soc. Jpn.* **2013**, *82*, 123705.
[33] A. Coelho. TOPAS-Academic, Version 4.1, Coelho Software. Brisbane, **2007**.
[34] V. Petricek, M. Dusek, L. Palatinus. Jana2006. structure determination software programs, **2009**.
[35] G. Kresse, J. Hafner, *Phys. Rev. B* **1994**, *49*, 14251.
[36] G. Kresse, J. Furthmüller, *Comput. Mater. Sci.* **1996**, *6*, 15.
[37] P. E. Blöchl, *Phys. Rev. B* **1994**, *50*, 17953.
[38] J. P. Perdew, K. Burke, M. Ernzerhof, *Phys. Rev. Lett.* **1996**, *77*, 3865.

  